Passive Q-switching of Yb:CNGS lasers by Cr^{4+}:YAG and V^{3+}:YAG saturable absorbers

Xuzhao Zhang,[1,2] Pavel Loiko,[3] Josep Maria Serres,[1] Venkatesan Jambunathan,[4] Zhengping Wang,[2,7] Shiyi Guo,[2] Anatoly Yasukevich,[5] Antonio Lucianetti,[4] Tomas Mocek,[4] Uwe Griebner,[6] Valentin Petrov,[6] Xinguang Xu,[2,8] Magdalena Aguiló,[1] Francesc Díaz,[1] and Xavier Mateos[1,*]

[1]Universitat Rovira i Virgili, Departament Química Física i Inorgànica, Física i Cristal·lografia de Materials i Nanomaterials (FiCMA-FiCNA)-EMaS, Campus Sescelades, E-43007, Tarragona, Spain.
[2]State Key Laboratory of Crystal Materials and Institute of Crystal Materials, Shandong University, 250100 Jinan, China
[3]ITMO University, 49 Kronverkskiy pr., 197101 St. Petersburg, Russia
[4]HiLASE Centre, Institute of Physics of the Czech Academy of Sciences, Za Radnicí 828, 25241 Dolní Břežany, Czech Republic
[5]Center for Optical Materials and Technologies (COMT), Belarusian National Technical University, 65/17 Nezavisimosti Ave., 220013 Minsk, Belarus
[6]Max Born Institute for Nonlinear Optics and Short Pulse Spectroscopy, Max-Born-Str. 2a, D-12489 Berlin, Germany
[7]zpwang@sdu.edu.cn
[8]xgxu@sdu.edu.cn
**Corresponding author: xavier.mateos@urv.cat*

Received XX Month XXXX; revised XX Month, XXXX; accepted XX Month XXXX; posted XX Month XXXX (Doc. ID XXXXX); published XX Month XXXX

Trigonal langasite-type ordered silicate crystal Yb:$Ca_3NbGa_3Si_2O_{14}$ (Yb:CNGS) is a promising material for efficient ~1 μm lasers. We report on the first passively Q-switched Yb:CNGS laser using Cr^{4+}:YAG and V^{3+}:YAG saturable absorbers (SAs) with a 976 nm Volume Bragg Grating (VBG)-stabilized diode as a pump source. The laser crystal was a *c*-cut 3 at.% Yb:CNGS grown by the Czochralski method. It was placed in a compact microchip-type laser cavity. With a Cr^{4+}:YAG SA, very stable 62.2 μJ / 4.4 ns pulses were achieved at a repetition rate of 22.5 kHz. The average output power was 1.40 W at 1015.3 nm corresponding to a Q-switching conversion efficiency of 90%. With the V^{3+}:YAG SA, the pulse characteristics were 13.3 μJ / 11.1 ns at a higher repetition rate of 68.4 kHz. The performance of the Yb:CNGS/Cr^{4+}:YAG was numerically modelled showing a good agreement with the experiment.

OCIS codes: *(140.3070) Infrared and far-infrared lasers; (140.3540) Lasers, Q-switched; (140.3380) Laser materials.*

http://dx.doi.org/10.1364/AO.99.099999

1. Introduction

Passive Q-switching is a commonly used approach to generate nanosecond (ns) pulses from diode-pumped solid-state lasers (DPSSLs) [1,2]. It is realized by the insertion of a nonlinear optical element, saturable absorber (SA), into the laser cavity. Passively Q-switched (PQS) DPSSLs possess the advantages of all-solid, compact and external-control-free design, as compared to the actively Q-switched ones. Passive Q-switching can also be implemented for microchip lasers where the active element (AE) and the SA are placed in a compact plano-plano cavity potentially resulting in sub-ns pulse durations [3-5].

The SAs can be classified as "slow" and "fast" according to the relation between the recovery time of their initial absorption, τ_{rec}, and the characteristic time of the pulse formation, ΔT, namely $\tau_{rec} >> \Delta T$ and $\tau_{rec} << \Delta T$, respectively. "Slow" SAs in particular are useful to achieve high pulse energies (up to mJ), short pulse durations (down to sub-ns) and high peak powers (up to MW) from PQS DPSSLs. Typically, "slow" SAs are based on crystals doped with transition-metal (TM) ions located in tetrahedral (T_d) sites and thus featuring high transition cross-sections [6]. This leads to low saturation fluence and easier bleaching of such SAs. For example, in the spectral region of ~1 μm (Nd^{3+} and Yb^{3+} lasers), such a state-of-the-art "slow" SA is Cr^{4+}-doped $Y_3Al_5O_{12}$ (YAG) [7,8]. The niche of "fast" SAs (e.g., Semiconductor

Saturable Absorber Mirrors, SESAMs) is the high-repetition-rate (up to MHz) PQS lasers exhibiting small (few μJ) pulse energies [9].

During the last decades, the interest in ~1 μm lasers has shifted from Nd^{3+} to Yb^{3+} ion doping [10]. This is because the Yb^{3+} ion possesses a simple energy level scheme allowing for a high Stokes efficiency, eliminating parasitic processes like upconversion and thus leading to a weak heat loading and high laser slope efficiency. The Yb^{3+} ion typically has longer lifetime of the upper-state, $^2F_{5/2}$ (as compared to that for Nd^{3+}) which is desirable for energy storage in PQS operation.

Ordered trigonal (langasite-type) calcium niobium gallium silicate crystal $Ca_3NbGa_3Si_2O_{14}$ (shortly CNGS) has been recognized recently as a promising host for Yb^{3+} doping [11]. This host crystal features good thermal, mechanical and elastic properties [11-13] leading to a high thermal fracture limit and good power scaling capabilities, as well as high Yb^{3+} doping levels (up to 5 at.%). Large-volume high-optical-quality CNGS crystals can be grown by the standard Czochralski (Cz) method [12]. The Yb^{3+} ion in CNGS exhibits high transition cross-sections and relatively long upper-level lifetime of 710 μs [14]. Moreover, the non-centrosymmetric CNGS (point group 32) can be used as a self-frequency-doubling (SFD) material [15].

To date, the research on Yb:CNGS has focused on its growth, structure, spectroscopic and continuous-wave (CW) laser properties [14,16]. In [16] under diode-pumping at 976 nm, a 3 at.% Yb:CNGS laser generated 7.61 W of CW output at 1048-1060 nm with a slope efficiency of 59%. In [11], a type I-cut 5 at.% Yb:CNGS CW SFD laser was demonstrated delivering 37 mW of green output at 530 nm.

In the present work, we demonstrate the first PQS Yb:CNGS laser using two TM-ion doped crystal SAs, Cr^{4+}:YAG and V^{3+}:YAG [17]. This can be considered as a first step towards green ns SFD Yb:CNGS lasers.

2. Experimental

The scheme of the laser set-up is shown in Fig. 1. The pump source was a VBG-stabilized fiber-coupled InGaAs laser diode (BWT Beijing LTD, fiber core diameter: 105 μm; numerical aperture, N.A.: 0.22) delivering up to ~27 W of unpolarized output at 975.8 nm (emission bandwidth: 0.6 nm, M^2 = 36). The pump radiation was collimated and focused into the active element (AE) by a lens assembly (1:1 imaging ratio, focal length: 30 mm). This resulted in a beam spot radius w_p of 52 μm and a Rayleigh length of $2z_R$ = 1.0 mm (in the AE).

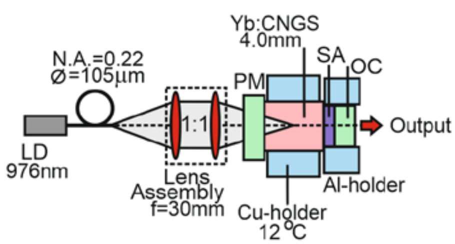

Fig. 1. Scheme of the PQS Yb:CNGS microchip laser: LD – VBG-stabilized InGaAs laser diode, PM – pump mirror, OC – output coupler (both flat), SA – saturable absorber (Cr^{4+}:YAG or V^{3+}:YAG, AR-coated).

The AE was prepared from a *c*-cut 3 at.% Yb:CNGS crystal (N_{Yb} = 3.2×10^{20} cm^{-3}) grown by the Czochralski method [11]. This crystal cut offers higher pump absorption and provides access to the high-gain σ-polarization. The AE was 4 mm-thick with an aperture 3(*a*)×3 mm^2, polished to laser quality and uncoated. The AE was mounted in a Cu-holder providing cooling from all 4 lateral sides of the crystal and indium foil was used to improve the thermal contact. The holder was water-cooled to 12 °C.

The spectroscopic properties the of 3 at.% Yb:CNGS crystal are shown in Fig. 2 (σ-polarization). The maximum absorption cross-section, σ_{abs}, is 1.25×10^{-20} cm^2 at 977.0 nm corresponding to a full width at half maximum (FWHM) of 4.6 nm, Fig. 2(a). The maximum stimulated-emission (SE) cross-section, σ_{SE}, in the long-wavelength spectral range where laser operation is expected is 0.97×10^{-20} cm^2 at 1014 nm. In Fig. 2(b), we also show the gain cross-sections, $\sigma_g = \beta\sigma_{SE} - (1 - \beta)\sigma_{abs}$, where $\beta = N_2(^2F_{5/2})/N_{Yb}$ is the inversion ratio. For high β > 0.15, laser operation is expected around the local peak in the σ_g spectra at ~1014 nm.

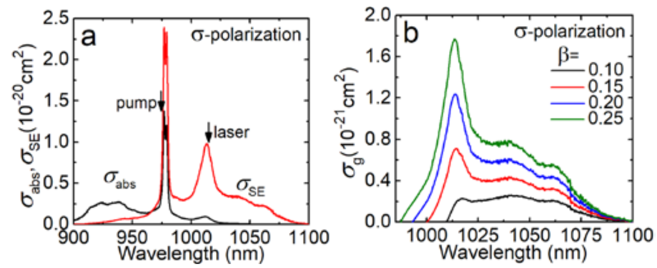

Fig. 2. (a,b) Spectroscopy of 3 at. % Yb:CNGS: (a) absorption, σ_{abs}, and stimulated-emission, σ_{SE}, cross-sections; (b) gain cross-sections, $\sigma_g = \beta\sigma_{SE} - (1 - \beta)\sigma_{abs}$ (for σ-polarization), $\beta = N_2(^2F_{5/2})/N_{Yb}$ is the inversion ratio. *Arrows* in (a) indicate the pump and laser wavelengths.

The AE was placed in a compact plano-plano (microchip-type) laser cavity. It was composed by a flat pump mirror (PM) coated for high transmission (HT) at 0.78-0.99 μm and high reflection (HR) at 1.01-1.23 μm, and a flat output coupler (OC) having a transmission T_{OC} = 30% at 1.02-1.20 μm. This T_{OC} value was selected to avoid damage of the optical components in the PQS operation mode. The AE was placed close to the PM. The SA and the OC (both having a diameter of 5 mm) were mounted together in a passively-cooled Al holder. This holder reduced the effect of the SA heating by the residual (non-absorbed) pump. The SA/OC stack was placed close to the AE, so that the geometrical cavity length L_{cav} was equal to $t_{AE} + t_{SA}$. Such a compact design was used to reduce the cavity round-trip time and to shorten the pulse duration in the PQS operation mode.

The AE was pumped through the PM. As the OC provided partial reflection at the pump wavelength (~70%), the crystal was pumped in a double-pass. The total pump absorption under lasing conditions was 58%. The radius of the laser mode in the AE was estimated with ABCD formalism as $w_L \approx 45\pm5$ μm.

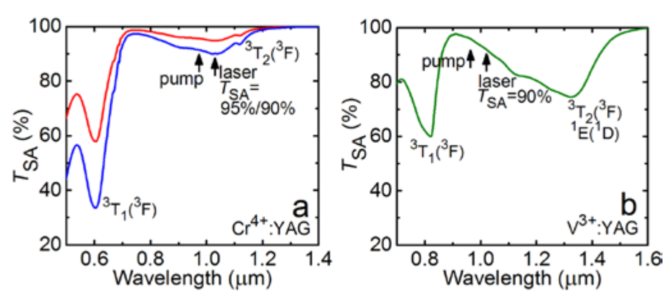

Fig. 3. Internal small-signal transmission, T_{SA}, of (a) two Cr^{4+}:YAG SAs with different thickness and (b) one V^{3+}:YAG SA. *Arrows* indicate the pump and laser wavelengths.

Two types of the SA were used based on the Cr^{4+}:YAG and V^{3+}:YAG crystals. They were polished to laser-grade quality and antireflection (AR) coated for 1.02-1.04 μm on both sides. Two Cr^{4+}:YAG SAs having different thickness were used. Their initial (small-signal) transmission was T_{SA} = 95% (thickness, t_{SA} = 1.45 mm) or 90% (t_{SA} = 1.55 mm). One V^{3+}:YAG SA provided T_{SA} of 90% (t_{SA} = 0.83 mm). Here, T_{SA} is specified at the laser wavelength. The internal (uncoated, subtracting Fresnel reflection) small-signal transmission spectra of the three studied SAs are shown in Fig. 3. For Cr^{4+}:YAG, the laser wavelength overlaps with the center of the broad 0.8-1.25 µm absorption band due to the $^3A_2(^3F) \rightarrow {}^3T_2(^3F)$ transition of the Cr^{4+} ions in T_d sites [18]. The corresponding ground-state absorption (GSA) cross-section, $\sigma_{GSA} = 4.5\times10^{-18}$ cm^2 and the saturation contrast, $\gamma = \sigma_{ESA}/\sigma_{GSA} \sim 0.2$ (ESA – excited-state absorption) [5]. For V^{3+}:YAG, the laser wavelength corresponds to the short-wavelength edge of a broad 0.9-1.6 µm band due to the $^3A_2(^3F) \rightarrow {}^3T_2(^3F) + {}^1E(^1D)$ transition of V^{3+} ions in T_d sites. The corresponding $\sigma_{GSA} = 2.5\times10^{-18}$ cm^2 and $\gamma = \sigma_{ESA}/\sigma_{GSA} \sim 0.2$ [17].

The Q-switched pulses were recorded by a 2 GHz digital oscilloscope and a fast InGaAs photodiode with 200 ps rise time. The laser emission spectra were measured with a compact spectrometer (APE GmbH, WaveScan, resolution: 0.2 nm).

3. Results and discussion

Trigonal CNGS is an optically uniaxial crystal. Its optical axis is parallel to the *c*-axis. The principal refractive indices at ~1 µm are n_o = 1.772 and n_e = 1.855 [19] (a positive uniaxial crystal). For a *c*-cut Yb:CNGS, any wave propagating along the AE axis will correspond to σ-polarization so that the laser output will be partially polarized.

At first, we studied the CW performance of the Yb:CNGS laser (without a SA in the cavity), Fig. 4. The maximum output power was 1.76 W at 1015-1017 nm (a multi-peak emission due to etalon effects) with a slope efficiency η of 16% (with respect to the absorbed pump power, P_{abs}). The laser threshold was at P_{abs} = 2.5 W and the optical-to-optical efficiency η_{opt} was 7.5% (with respect to the incident pump power). The input-output dependence was linear up to at least P_{abs} = 13.6 W indicating negligible thermal effects. Note that the reduced slope efficiency as compared to Ref. [16] is due to a much higher output coupling used in the present work (T_{OC} = 30%) which was needed to ensure stable PQS operation.

By inserting the SAs in the laser cavity, very stable Q-switching was achieved. The corresponding output dependences are shown in Fig. 4. For all SAs, there was a lower limit of Q-switching stability near the threshold. For P_{abs} > 12.3 W, although the stability was preserved, the average output power was not increasing due to excessive heating of the SA.

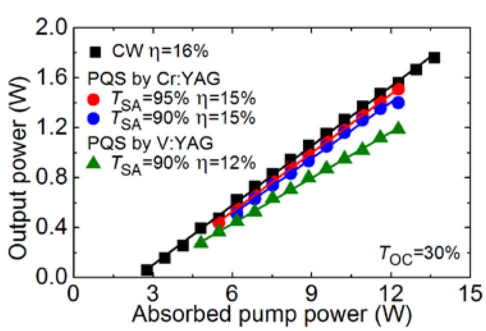

Fig. 4. Input-output dependences for CW and PQS Yb:CNGS microchip lasers using Cr^{4+}:YAG and V^{3+}:YAG SAs: η – slope efficiency, T_{SA} – initial transmission of the SA.

The maximum average output power (P_{out}) corresponded to Cr^{4+}:YAG SA with T_{SA} = 95%, namely 1.51 W at 1015.8 nm with η = 15% and a conversion efficiency with respect to the CW mode η_{conv} = 97%. For the same type of SA with T_{SA} = 90%, the output power was slightly lower, 1.40 W at 1015.3 nm with η = 15%, and η_{conv} was reduced to 90%. This reduction originates from the higher insertion loss for this SA. For V^{3+}:YAG SA, the laser performance was inferior: The PQS laser generated 1.19 W at 1015.1 nm with η = 12% and η_{conv} = 76%. The achieved high Q-switching conversion efficiency is due to the AR coating of the SAs and the compact cavity design.

Typical laser spectra for CW and PQS Yb:CNGS lasers are shown in Fig. 5. The emission is at ~1015 nm in agreement with the gain spectra, Fig. 2(b). The spectra of the PQS lasers consist of a single narrow (< 0.3 nm) peak contrary to the multi-peak emission of the CW laser. This is typical for PQS lasers where only the strongest laser line saturates the SA [1]. The laser wavelength experienced a blue-shift when going from CW mode to passive Q-switching with Cr^{4+}:YAG and further with V^{3+}:YAG indicating increased intracavity losses due to the insertion of the SA. This is due to the quasi-three level nature of the Yb^{3+} laser.

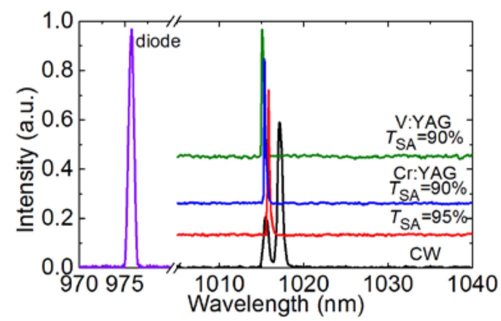

Fig. 5. Typical laser emission spectra for the CW and PQS Yb:CNGS microchip lasers using Cr^{4+}:YAG and V^{3+}:YAG SAs measured at P_{abs} = 12.3 W; the spectrum of the VBG-stabilized InGaAs laser diode is shown for comparison. T_{SA} – initial transmission of the SA.

The pulse repetition frequency (PRF) and duration, $\Delta\tau$, (determined as FWHM) were measured directly and the pulse energy E_{out} and peak power P_{peak} were calculated as $E_{out} = P_{out}$/PRF and $P_{peak} = E_{out}/\Delta\tau$. The results on these pulse characteristics are shown in Fig. 6.

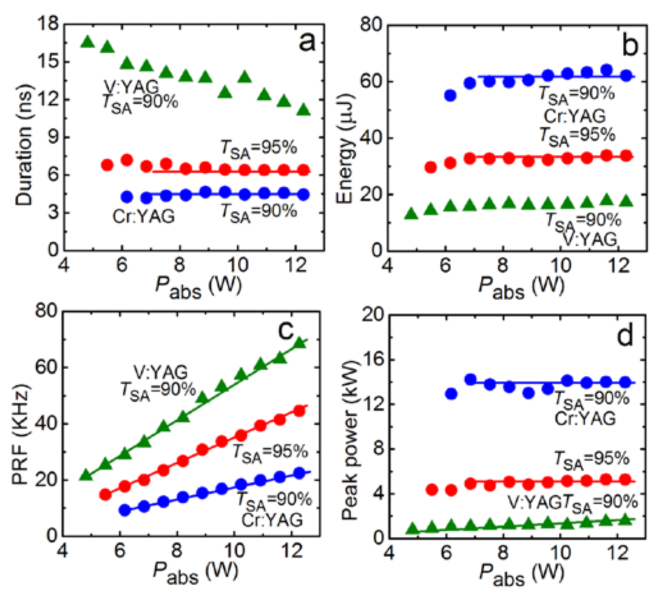

Fig. 6. (a-d) Microchip Yb:CNGS laser PQS by Cr^{4+}:YAG and V^{3+}:YAG SAs: (a) pulse duration (FWHM), (b) pulse energy, (c) pulse repetition frequency (PRF), (d) peak power. T_{SA} – initial transmission of the SA. *Horizontal lines* in (a,b,d) for Cr^{4+}:YAG SA – average values of the pulse characteristics, *lines* in (c) – linear fits of the PRF vs. P_{abs} dependence.

Cr^{4+}:YAG is a "slow" SA for Yb^{3+} lasers. The lifetime of the $^3T_2(^3F)$ state of Cr^{4+} ions, which determines the recovery time of the initial absorption τ_{rec} is about 3.4 µs [5,6] which is much longer than the characteristic time of the formation of a Q-switched pulse (few ns). For such "slow" SAs, there is a criterion of efficient Q-switching, $X = A_{mode}\times[\sigma_{GSA} - \sigma_{ESA}]/[\sigma^{L}_{SE} + \sigma^{L}_{abs}] >> 1$ [20]. Here, A_{mode} is the ratio of mode areas in the AE and SA, which is ~1 in microchip lasers [5], σ^{L}_{SE} and σ^{L}_{abs} are the SE and reabsorption cross-sections for the AE at the laser wavelength. When $X >> 1$, the pulse characteristics (energy and duration) are weakly dependent on the pump power. For the designed Yb:CNGS/Cr^{4+}:YAG laser, $X \approx 350$. Indeed, the pulse energy/duration are almost constant for both Cr^{4+}:YAG SAs, see Fig. 6(a,b), amounting to 33.8 μJ / 6.4 ns (for T_{OC} = 95%) and 62.2 μJ / 4.4 ns (for T_{OC} = 90%) at P_{abs} = 12.3 W. As a result, the PRF shows a linear dependence on the pump power, Fig. 6(c), varying from 14.8 to 44.6 kHz (for T_{OC} = 95%) and from 9.3 to 22.5 kHz (for T_{OC} = 90%). The peak power, in turn, is also almost pump-independent, Fig. 6(d), amounting to 5.3 and 14.0 kW (T_{OC} = 95% and 90%, respectively) at the maximum P_{abs} = 12.3 W.

For V^{3+}:YAG, τ_{rec} = 22 ns [17]. Consequently, this material takes an intermediate place between "slow" and "fast" SAs for Yb^{3+} lasers. This is revealed in a dependence of the pulse characteristics on P_{abs}. For our microchip laser, due to the short cavity round-trip time, τ_{rec} is longer than the characteristic time of the pulse formation, so V^{3+}:YAG behaves more like a "slow" SA and the above-mentioned dependence is weak as compared, e.g., with such "fast" SAs as SESAM [9]. With the increase of P_{abs}, $\Delta\tau$ is shortened from 16.5 to 11.1 ns and E_{out} increases from 12.8 to 17.3 μJ. The PRF increases almost linearly from 21.3 to 68.4 kHz and the maximum peak power is 1.56 kW.

The oscilloscope traces of the shortest Q-switched pulses for all three studied SAs are shown in Fig. 7. The pulses have a nearly-Gaussian temporal shape.

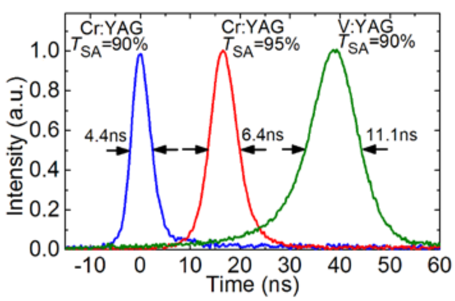

Fig. 7. Oscilloscope traces of the shortest Q-switched pulses achieved from Yb:CNGS microchip lasers PQS by Cr^{4+}:YAG and V^{3+}:YAG SAs (at P_{abs} = 12.3 W). T_{SA} – initial transmission of the SA.

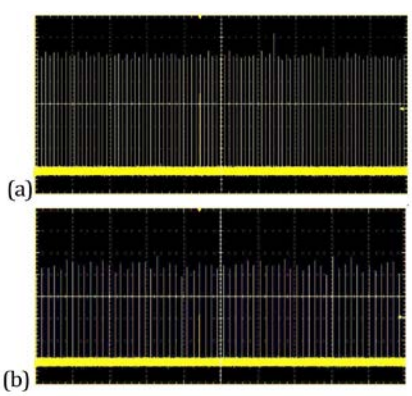

Fig. 8. Oscilloscope traces of the pulse trains from the Yb:CNGS microchip lasers PQS by (a) Cr^{4+}:YAG SA (T_{SA} = 95%, at P_{abs} = 11.6 W) and (b)V^{3+}:YAG SA (T_{SA} = 90%, at P_{abs} = 10.2 W). The PRF is 41 kHz (a) and 56 kHz (b). The total time span is 2 ms (a) and 1 ms (b).

Typical oscilloscope traces of the pulse trains from the Yb:CNGS lasers PQS by Cr^{4+}:YAG and V^{3+}:YAG SAs are shown in Fig. 8. For these SAs, the intensity instabilities in the pulse train are <7% (<10%) and the root-mean-square (rms) pulse-to-pulse timing jitter is <10% (<15%), respectively.

Table 1 Output Characteristics* of the PQS Yb:CNGS Lasers

SA	T_{SA}, %	P_{out}, W	η, %	E_{out}, μJ	$\Delta\tau$, ns	PRF, kHz	P_{peak}, kW	η_{conv}, %
Cr^{4+}:YAG	95	1.51	15	33.8	6.4	44.6	5.3	97
	90	1.40	15	62.2	4.4	22.5	14.0	90
V^{3+}:YAG	90	1.19	12	17.3	11.1	68.4	1.56	76

*T_{SA} – initial transmission of the SA, P_{out} – average output power, η – slope efficiency, E_{out} –pulse energy, $\Delta\tau$ – pulse duration, PRF – pulse repetition frequency, P_{peak} – peak power, η_{conv} – conversion efficiency with respect to the CW mode.

Both CW and PQS Yb:CNGS lasers generated almost diffraction-limited circular output beam with a measured $M^2_{x,y} < 1.2$.

The output characteristics of the PQS Yb:CNGS lasers are summarized in Table 1.

During the PQS operation, no damage of the SA was observed. The axial intracavity fluence at the SA, calculated as $F_{in} = Y[2E_{out}/\pi w_L^2]$ where $Y = (2 - T_{OC})/T_{OC}$ and the term "2" indicates a Gaussian spatial profile of the laser mode [21], amounted to 6.0 and 11.1 J/cm² (for Cr^{4+}:YAG SAs with T_{SA} = 95% and 90%, respectively) and 3.1 J/cm² (for V^{3+}:YAG SA). This is below the laser-induced damage threshold (LIDT) for AR-coated YAG, ~20 J/cm². However, these values of F_{in} are well above the saturation fluence, $F_S = h\nu_L/\sigma_{GSA}$ = 0.04 J/cm² (for Cr^{4+}:YAG) and 0.08 J/cm² (for V^{3+}:YAG) resulting in complete bleaching of these SAs.

Table 2 Material Parameter of the Yb:CNGS Laser Crystal and Cr^{4+}:YAG SA Used for the Calculations

Parameter	Notation	Value
Laser crystal*: Yb^{3+}:CNGS		
Yb^{3+} concentration	N_{Yb}	3.2×10^{20} cm^{-3}
SE cross-section	σ^{L}_{SE}	0.97×10^{-20} cm²
Reabsorption cross-section	σ^{L}_{abs}	0.12×10^{-20} cm²
Lifetime of Yb^{3+} ion [14]	$\tau_{Yb}(^2F_{5/2})$	710 μs
Refractive index [19]	n_o	1.772
SA: Cr^{4+}:YAG [5,6]		
Ground/excited-state absorption cross-section	σ_{GSA} / σ_{ESA}	4.5×10^{-18} cm² / ~1×10^{-18} cm²
Saturation fluence	$F_S=h\nu_L/\sigma_{GSA}$	0.04 J/cm²
Recovery time	$\tau(^3T_2)$	3.4 μs
Refractive index	n_{SA}	1.816

*For σ-polarization

We have modelled the Q-switched performance of the Yb:CNGS / Cr^{4+}:YAG laser using a model of a quasi-three-level laser PQS by a "slow" SA [5,22]. The used material parameters of the AE and SA are listed in Table 2. The modelling results are plotted in Fig. 9 for E_{out} and $\Delta\tau$. With the increase of T_{OC}, the pulse energy increases and its duration is shortened while these dependences are saturated for T_{OC} > 30%. This explains additionally the selection of this OC. The modelling predicts the generation of 36 μJ / 6.4 ns and 64 μJ / 3.2 ns pulses for T_{OC} = 95% and 90%, respectively, which is in good agreement with the experiment.

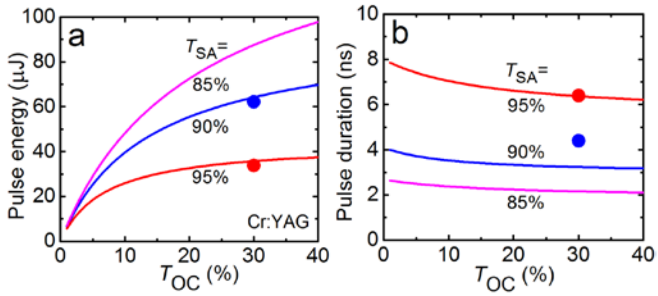

Fig. 9. (a,b) Modelling of the Yb:CNGS/Cr^{4+}:YAG PQS microchip lasers: calculated pulse energy (a) and duration (b) vs. transmission of the output coupler, T_{OC}, for various initial transmissions of the SA, T_{SA} (*curves*). *Symbols* – experimental data.

4. Conclusions

To conclude, we report on the first PQS Yb:CNGS lasers using two SAs for ~1 μm, namely Cr^{4+}:YAG and V^{3+}:YAG crystals. Trigonal Yb:CNGS silicate crystal is an attractive material for passive Q-switching owing to its good mechanical properties and energy storage ability (τ_{Yb} = 710 μs). By applying a VBG-stabilized 976 nm laser diode for efficient pump absorption, a microchip-type design for the short cavity round-trip time and AR-coated / passively-cooled SA diminishing the Q-switching instabilities, we demonstrated very stable Q-switching with an average output power of >1 W at ~1015 nm. The best pulse characteristics (energy/duration) were obtained using a Cr^{4+}:YAG SA with an initial transmission of 90%, namely 62.2 μJ / 4.4 ns at a repetition rate of 22.5 kHz corresponding to a peak power of 14 kW and a Q-switching conversion efficiency as high as 90%.

Further scaling of the pulse energy in PQS Yb:CNGS lasers seems feasible in extended-cavity or microchip configurations allowing for larger mode size w_L in the AE. In our case, w_L was limited by the small pump spot size and the thermal lens. In this way, pulse energies up to mJ-level may be obtained. As Yb:CNGS is a SFD material, compact PQS nanosecond green lasers can be developed based, e.g., on type I-cut AEs.

Funding Information. Spanish Government (MAT2016-75716-C2-1-R, (AEI/FEDER,UE), MAT2013-47395-C4-4-R, TEC 2014-55948-R); Generalitat de Catalunya (2017SGR755); National Natural Science Foundation of China (51472147, 61178060, 51672161). This article was co-financed by the European Regional Development Fund and the state budget of the Czech Republic (project HiLASE CoE: Grant No. CZ.02.1.01/0.0/0.0/15_006/0000674) and by the European Union's Horizon 2020 research and innovation programme under grant agreement No. 739573. This work was also supported by the Ministry of Education, Youth and Sports of the Czech Republic (Programmes NPU I Project No. LO1602, and Large Research Infrastructure Project No. LM2015086).

Acknowledgments. F.D. acknowledges additional support through the ICREA academia award 2010ICREA-02 for excellence in research. P.L. acknowledges financial support from the Government of the Russian Federation (Grant 074-U01) through ITMO Post-Doctoral Fellowship scheme.

References

1. J. Liu, V. Petrov, H. Zhang, and J. Wang, “Power scaling of a continuous-wave and passively Q-switched Yb:KLu$(WO_4)_2$ laser end-pumped by a high-power diode,” Appl. Phys. B **88**(4), 527-530 (2007).
2. H. Yu, V. Petrov, U. Griebner, D. Parisi, S. Veronesi, and M. Tonelli, "Compact passively Q-switched diode-pumped Tm:$LiLuF_4$ laser with 1.26 mJ output energy," Opt. Lett. **37**(13), 2544-2546 (2012).
3. J. J. Zayhowski and C. Dill, "Diode-pumped passively Q-switched picosecond microchip lasers," Opt. Lett. **19**(18), 1427-1429 (1994).
4. J. Dong, K. Ueda, A. Shirakawa, H. Yagi, T. Yanagitani, and A. A. Kaminskii, “Composite Yb:YAG/Cr^{4+}:YAG ceramics picosecond microchip lasers,” Opt. Express **15**(22), 14516-14523 (2007).
5. P. Loiko, J. M. Serres, X. Mateos, K. Yumashev, A. Yasukevich, V. Petrov, U. Griebner, M. Aguiló, and F. Díaz, “Sub-nanosecond Yb:KLu$(WO_4)_2$ microchip laser,” Opt. Lett. **41**(11), 2620–2623 (2016).
6. A. M. Malyarevich and K. V. Yumashev, “Saturable absorbers based on tetrahedrally coordinated transition-metal ions in crystals,” J. Appl. Spectr. **76**(1), 1-43 (2009).
7. A. Agnesi, S. Dell'Acqua, C. Morello, G. Piccinno, G. C. Reali, and Z. Sun, “Diode-pumped neodymium lasers repetitively Q-switched by Cr^{4+}:YAG solid-state saturable absorbers,” IEEE J. Sel. Top. Quantum Electron. **3**(1), 45-52 (1997).
8. Y. Kalisky, C. Labbe, K. Waichman, L. Kravchik, U. Rachum, P. Deng, J. Xu, J. Dong, and W. Chen, “Passively Q-switched diode-pumped Yb:YAG laser using Cr^{4+}-doped garnets,” Opt. Mater. **19**(4), 403-413 (2002).
9. G. J. Spühler, R. Paschotta, R. Fluck, B. Braun, M. Moser, G. Zhang, E. Gini, and U. Keller, "Experimentally confirmed design guidelines for passively Q-switched microchip lasers using semiconductor saturable absorbers," J. Opt. Soc. Am. B **16**(3), 376-388 (1999).
10. W. F. Krupke, “ Ytterbium solid-state lasers. The first decade,” IEEE J. Sel. Top. Quantum Electron. **6**(6), 1287-1296 (2000).
11. X. Zhang, Y. Zhou, J. Ren, D. Lu, H. Yu, Z. Wang, S. Guo, and X. Xu, “Growth, thermal and laser properties of a new self-frequency doubling Yb:CNGS crystal,” Cryst. Eng. Comm. **18**(28), 5338-5343 (2016).
12. Z. M. Wang, X. F. Cheng, D. R. Yuan, L. H. Pan, S. Y. Guo, D. Xu, and M. K. Lv, “Crystal growth and properties of $Ca_3NbGa_3Si_2O_{14}$ single crystals,” J. Cryst. Growth **249**(1-2), 240–244 (2003).
13. I. H. Jung, A. Yoshikawa, T. Fukuda, and K. H. Auh, “Growth and structure of $A_3NbGa_3Si_2O_{14}$ (A = Sr, Ca) compounds,” J. Alloy Compd. **339**(1-2), 149-155 (2002).
14. X. Zhang, P. Loiko, J.M. Serres, X. Mateos, J. Ren, Z. Wang, S. Guo, X. Xu, E. Vilejshikova, U. Griebner, V. Petrov, M. Aguiló, and F. Díaz, “Highly-efficient laser operation of a novel trigonal silicate crystal - Yb^{3+}:$Ca_3NbGa_3Si_2O_{14}$,” Opt. Mater. Express **7**(10) 3626-3633 (2017).
15. X. Zhang, Y. Zhou, A. Yasukevich, P. Loiko, X. Mateos, X. Xu, S. Guo, and Z. Wang, “Diode-pumped passively Q-switched self-frequency-doubled Nd:CNGS laser,” Opt. Express **25**(17), 19760-19766 (2017).
16. X. Zhang, P. Loiko, X. Mateos, J.M. Serres, J. Ren, J. Guo, R. Cheng, C. Gao, Q. Dong, V. Jambunathan, A. Lucianetti, T. Mocek, E. Vilejshikova, U. Griebner, V. Petrov, Z. Wang, S. Guo, X. Xu, M. Aguilo, and F. Diaz, “Crystal growth, low temperature spectroscopy and multi-watt laser operation of Yb:$Ca_3NbGa_3Si_2O_{14}$,” J. Lumin. **197**, 90-97 (2018).
17. A. M. Malyarevich, I. A.Denisov, K. V. Yumashev, V. P. Mikhailov, R. S. Conroy, and B. D. Sinclair, “V:YAG-a new passive Q-switch for diode-pumped solid-state lasers,” Appl. Phys. B **67**(5), 555-558 (1998).
18. Y. Kalisky, “Cr^{4+}-doped crystals: their use as lasers and passive Q-switches,” Prog. Quantum Electron. **28**(5), 249–303 (2004).
19. X. Zhang, X. Zhang, S. Guo, J. He, K. Han, F. Lou, B. Zhang, R. Wang, and X. Liu, "Growth and optical properties of a new CGG-type laser crystal Nd^{3+}:CNGS," Opt. Mater. Express **5**(5), 977-985 (2015).
20. A. E. Siegman, Lasers. Mill Valley, CA: Univ. Sci. Books, 1986, pp. 1024–1028.
21. S. Chénais, F. Balembois, F. Druon, G. Lucas-Leclin, and P. Georges, “Thermal lensing in diode-pumped ytterbium lasers-part II: evaluation of quantum efficiencies and thermo-optic coefficients,” IEEE J. Quantum Electron. **40**(9), 1235-1243 (2004).
22. J. M. Serres, P. A. Loiko, X. Mateos, V. Jambunathan, A. S. Yasukevich, K. V. Yumashev, V. Petrov, U. Griebner, M. Aguiló, and F. Díaz, “Passive Q-switching of Tm,Ho:KLu$(WO_4)_2$ microchip laser by a Cr:ZnS saturable absorber,” Appl. Opt. **55**(14), 3757-3763 (2016).